Raman spectroscopy study on the vibration and structural changes of graphene oxide: effect of laser power and time

S. Yadav[a], S. K. Padhi[b], Ch. Srinivasulu[c], K. L. Naidu[a,*]
[a]*Department of Physics, GSS, GITAM (Deemed to be University), Visakhapatnam, 530045, India*
[b]*Physics Department, University of Turin, Via. P. Giuria 1-710125 Turin, Italy.*
[c]*School Of Physics, University of Hyderabad, Hyderabad 500046, India.*

Graphene oxide and its nanocomposites play a crucial role in various applications. Laser irradiation is a low-cost technique to tune the graphene oxide material, and a detailed study of the vibrational modes and structural changes during the laser–graphene oxide interaction is required. The evolution of defect modes and reduction process in graphene oxide at varying laser power and different exposure time duration, respectively, via Raman spectroscopy, is of interest in the present study. Graphene oxide (GO) is synthesized via Improved Hummer's method and characterized by X-Ray Diffraction (XRD), Thermogravimetric analysis (TGA), Field Emission Scanning Electron Microscopy (FE-SEM), Energy Dispersive X-ray analysis (EDX), UV-Vis-NIR and Raman spectroscopy. The first-order Raman spectrum of GO consists of broad D and G peaks around 1350 and 1584 $cm^{-1,}$ respectively, and the broad second-order band around 2700 cm^{-1}. Using the Lorentzian function, the first-order band is deconvoluted into five modes and the second-order into four modes. The peak positions and FWHM of these modes undergo indicative changes. The variations in the intensity ratios of the defect modes and the $(D'_{inf} - G_{app})$ with laser power at different exposure time durations indicates the predominance of edge defects and reduction of graphene oxide, respectively. These results broaden the understanding of the effect of laser power over different time durations on the graphene oxide features. Our study provides quantitative information on the laser-GO interaction.

(Received January 21, 2024; Accepted April 8, 2024)

Keywords: Graphene oxide, Defects, Laser power, Raman spectroscopy, In-plane crystallite size (L_a)

1. Introduction

Graphene oxide is a two-dimensional functionalized-graphene sheet with oxygen-containing functional molecules attached at the edge and basal plane. Graphene oxide has been widely utilized in electrochemical supercapacitors [1], biomedical [2], sensors [3], field effect transistors (FET)[4], fuel cells [5], lithium batteries [6], polymer nanocomposites[7]. Different methods, including chemical, thermal, hydrothermal, electrochemical, and photochemical reduction, are developed to reduce the functional groups to achieve a graphene-like structure, well known as reduced graphene oxide. The ion doping technique has recently generated graphene oxide films with precise tuning and tailoring of defects by removal of unstable C=O bonds[8]

Raman spectroscopy analysis is a non-destructive tool to gain knowledge about defects and disorders apart from the structural information from the spectral parameters. The structural-spectral correlations were developed by quantifying the changes in the Raman spectra with the corresponding analysis of the X-ray diffraction pattern or X-ray photoelectron spectra of the samples [9–11]. The Raman spectra of graphene oxide contain the first-order band with characteristic peaks around 1350 (D-band) and 1580 cm^{-1}(G-band) and a broad second-order band around 2700 cm^{-1}. Generally, the G-band is characteristic of a graphene sheet, and the D-band evolves with an increase in the defects and disorders in the graphene sheet. The intensity ratio of

* Corresponding author: lakshun14@gmail.com
https://doi.org/10.15251/JOR.2024.202.221

cumulative I(D)/I(G) ratio for the case of Graphene oxide prepared via Improved Hummer's method fails to provide precise information about the defects and disorders, unlike situations where disorders are introduced in a controlled fashion [12]. It is claimed that only for crystallite size less than 2 nm the I(D)/I(G) can be related to the disorder. The knowledge of deconvoluted individual spectral modes of Raman spectra is required to avoid ambiguity in understanding the structural aspects of graphene oxide directly from the Raman spectra.

The G and D band arises due to the stretching of in-plane sp^2 carbon bonds in pairs and the breathing mode of individual sp^2 carbon atoms in rings, respectively. The double resonant process near the K point of the first Brillouin zone boundary primarily attributes to the D band. Apart from the G and D bands, three more bands, namely D*, D', and D" arises at positions about 1150,1350, and 1626 $cm^{-1,}$ respectively. The spectral parameters (intensity, position, Full width at Half maxima FWHM) of defect band D* correlates to the oxidation degree and show disorders due to the presence of sp3 bonds, similar to those in nanocrystalline diamonds where the defects correlate to the trans-polyacetylene groups[13]. The band D' is due to the intra-valley resonance with the G band, and the apparent G peak is the superposition of the D' and G bands. The position of D' correlates with the oxygen content [13,14].

Similarly, the decrease in intensity and width of defect band D" with the reduction process indicates the increase in the crystallinity of sheets. The D" is associated with the amorphous phases in graphene oxide. For the second order, Raman spectra centered at 2700 cm^{-1} indicate the number of layers; for example, a single layer shows a single peak, while a bilayer splits into four peaks. The four modes in the second-order Raman spectra are G*, 2D, D+D', and 2D' [15,16]. The G* mode is due to a double resonance intervalley process involving two phonons viz a longitudinal acoustic (LA) phonon and transverse optical (TO) phonon [16,17]. The 2D mode is an overtone of D mode due to the intervalley double resonance process. The D+D' mode is a two-phonon combination mode with different momenta near the Brillouin zone and requires defects for its activation. The 2D' mode is an overtone of the D' mode. Both the 2D and 2D' modes are activated even in the absence of defects [14,18–20].

The present study broadens the knowledge of different vibrational modes of graphene oxide and their evolution with laser power. The aim is to quantify all the first and second-order modes and relate them with the defects present. The study provides a complete picture of Raman modes in the first and second order, relative shifts in positions, and changes in in-plane crystallite size. The work is significant in observing the effects of laser power on the structural changes in graphene oxide. To the author's knowledge, no one has reported similar work.

2. Experimental

Chemical: Graphite fine powder, sulfuric acid, phosphoric acid, potassium permanganate, hydrogen peroxide, double distilled water, dilute hydrochloric acid, and ethanol are purchased from Loba chemicals and Merck and used as received.

Procedure: Graphene oxide is synthesized via the Improved Hummers method [21]. First, the required amount of graphite powder (1 wt. equivalent) was measured and added to the solution of H_2SO_4/H_3PO_4, taken in a 9:1 ratio. Then $KMnO_4$ (6 wt equivalent) is added slowly to the above solution. The whole setup was kept in an ice bath with continuous stirring overnight. Later, the solution is allowed to cool at room temperature and slowly poured on iced distilled water. Then the appropriate amount of H_2O_2 is added to terminate the reaction, confirmed through a change in color to yellow. The solution was centrifuged to obtain the required product and washed multiple times using double distilled water, 30% HCl, and ethanol twice, respectively. Then the material obtained after centrifuge was collected and dried in a hot air oven at 60˚C and named graphite oxide, which on sonication yields the graphene oxide.

Instrumentation: PANalytical X'Pert Pro for XRD. The Field Emission Scanning Electron Microscope (FESEM Model Ultra55 of Carl Zeiss) is used to conduct the microstructural analysis. The Agilent technologies Carry 5000 UV-Vis-NIR spectrophotometer used to determine the optical properties. Horiba Jobin Yvon at λ= 532 nm at different laser power is used in backscattering geometry to record the Raman spectroscopy. The accumulation time of the Raman spectra is 2s, recorded at laser power of 1, 10, 25, 50 and 100mW. The procedure is repeated for accumulation time of 5s.

3. Results

3.1. X-ray diffraction

The structural parameters are studied using X-ray diffraction, as shown in Fig. 1. The obtained pattern is analyzed using JCPDS file no. 00-008-0415. The XRD pattern of Graphite shows a sharp peak at 26.5° and some small peaks at 42.3°, 54.4°, 72.8°, and 77.3° corresponding to (002), (100), (110), (101), and (004) planes. The peaks at 10.3° correspond to the (001) plane of graphene oxide, as shown in Fig. 1b. The interplanar spacing d calculated using the Braggs law as mentioned below.

$$2dsin\theta = n\lambda$$

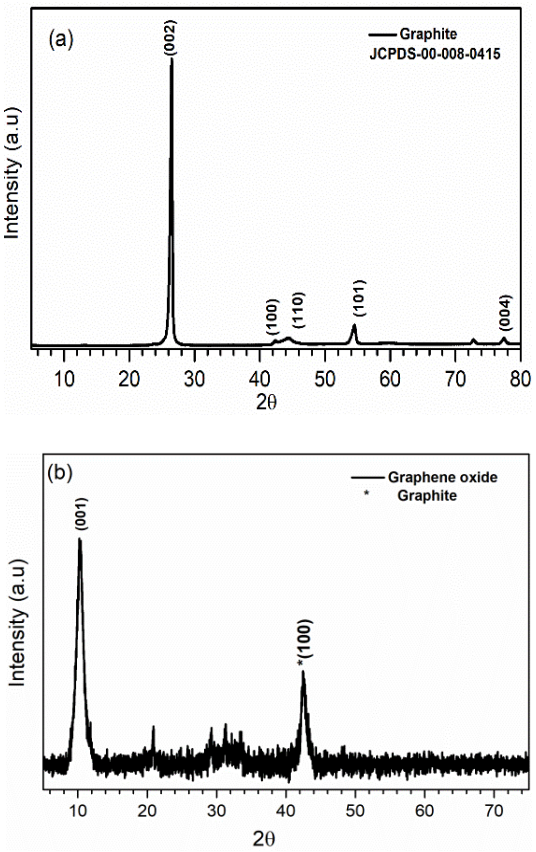

Fig. 1. XRD pattern of (a) graphite and (b) graphene oxide (GO).

The calculated value of d for Graphite is 3.35, 2.13, 1.68, 1.47, 1.23Å corresponding to (002), (100), (110), (101), and (004) planes, and for graphene oxide, interplanar spacing of 8.59Å corresponding to (001) plane, respectively.

3.2. Field Emission Scanning Electron Microscopy (FESEM)

The surface morphology of graphite and graphene oxide is observed through FESEM images at various magnifications, as shown in Fig. 2 and Fig. 3.

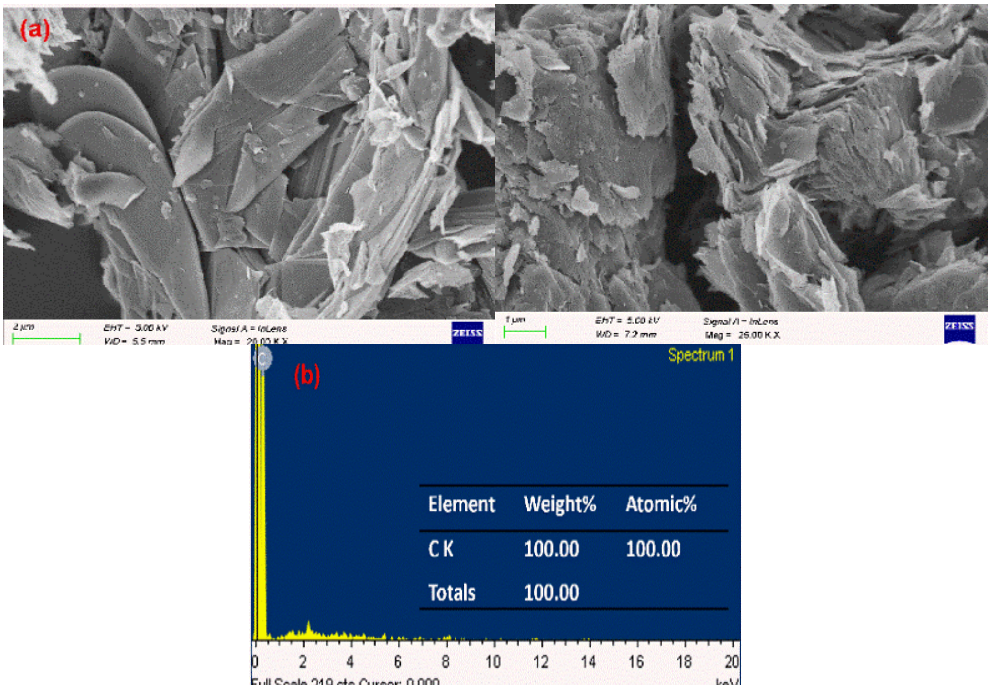

Fig. 2. (a) FESEM micrograph and (b) EDS of Graphite.

Fig. 2 represents the graphite image with non-uniform flakes-like structures stacked together in layer form and smooth surfaces. The Energy dispersive spectra (EDS) of Graphite show a pure 100 % C-k edge in both weight and atomic ratios.

The graphene oxide surface has been disrupted primarily due to chemical oxidation, and the ultrasonication treatment leads to breaking flakes into smaller particles, as shown in Fig. 3. The EDS of Graphene oxide shows a relative atomic ratio of 55% C and 45 % oxygen.

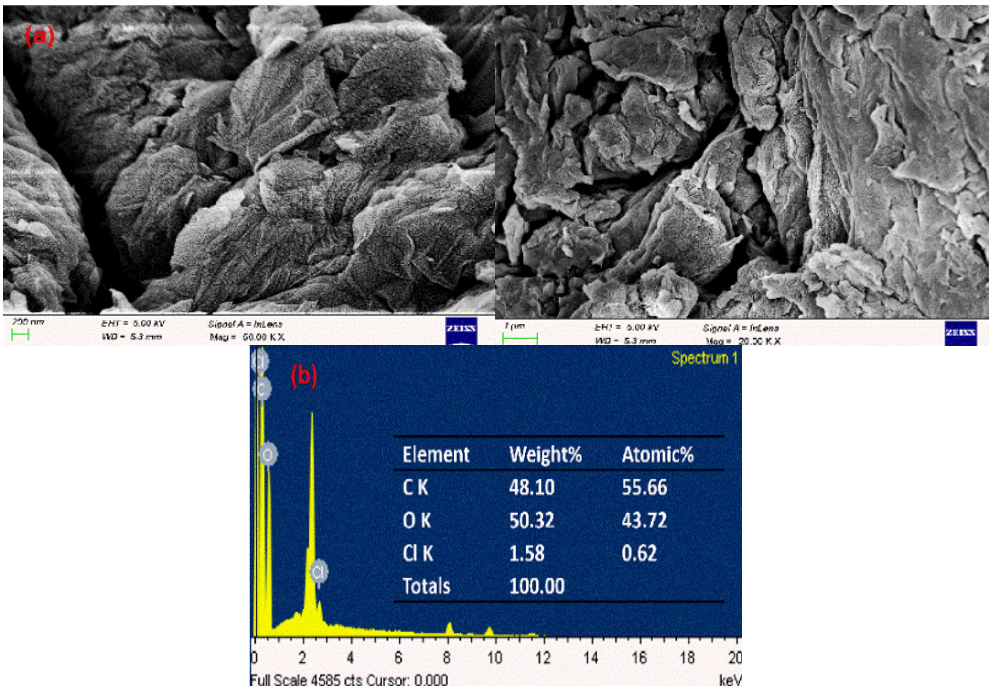

Fig. 3. (a) FESEM micrograph and (b) EDS of Graphene oxide.

3.3. Thermogravimetric analysis

The TGA-DTG graphs are plotted, showing the variation of mass loss with temperature change to study the thermal stability of graphite and graphene oxide. Fig. 4 shows that Graphite is more thermally stable than graphene oxide as mass loss is only 14% to 1000°C, whereas, for graphene oxide, mass loss occurs in three major stages.

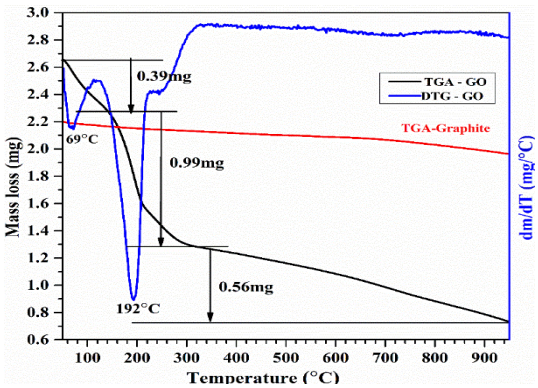

Fig. 4. TGA and DTG of GO in the range of 50 ℃ - 950 ℃.

In the first stage, 14% mass loss occurs due to the removal of water molecules at a temperature of less than 100°C. Then a rapid mass loss of 37% is observed between 100-300°C due to the pyrolysis of oxygen functional groups such as hydroxyl, carbonyl, and carboxyl groups from graphene oxide leading to the evolution of CO, CO_2, and H_2O. From 300°C to 900°C, about 21% mass loss occurs due to the combustion of carbon framework in the structure of graphene oxide[22]. Therefore, Graphite's maximum mass change rate at temperature Tmax is higher than graphene oxide. Graphene oxide has a high level of oxygen groups due to the oxidation process, thus requiring less heat to overcome the weaker sp^3 hybridized carbon atoms with high defect density. Graphite is the most thermodynamically stable carbon material which requires enormous heat to overcome the 3D network of graphene layers stacked together with van der Waals forces[23].

3.4. UV-VIS spectroscopy

Absorption spectra of graphene oxide are understood by UV-VIS spectroscopy, as shown in Fig. 5. The Fig. represents the characteristic peak at 230nm for graphene oxide corresponding to π-π* transition of aromatic carbon bonds.

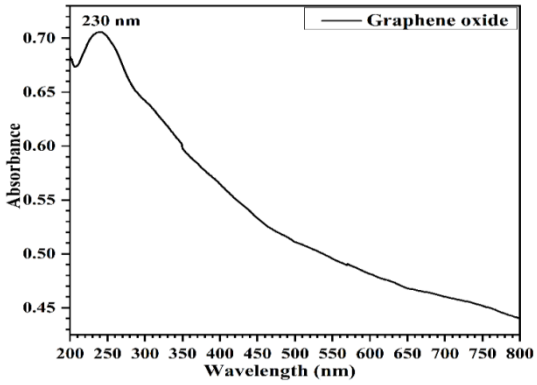

Fig. 5. UV-VIS spectroscopy of Graphene oxide.

The derivative of $(Abs/\lambda)^2$ is utilized to differentiate the higher and lower energy regions, namely, Tauc's and Urbach regions respectively. The band gap and Urbach energy obtained from the relations

$$Abs(\lambda) = B_1\lambda\left(\frac{1}{\lambda} - \frac{1}{\lambda g}\right)^m + B_2$$

where m=1/2 for allowed direct bandgap and m=2 for allowed indirect bandgap, and

$$Abs(\lambda) = D_3\, exp\left(\frac{hc}{E_{tail}\,\lambda}\right)$$

where E_{tail} is Urbach energy, explains the distribution of density of localized states of the allowed bands.

The plot between $(Abs/\lambda)^2$ and $1/\lambda$ as shown in Fig. 6, gives the optical band gap of 3.24 eV calculated from the Tauc region [24]. The Urbach energy calculation is done from the slope of the linear region of the graph plotted between Ln(abs) versus $1/\lambda$ and is calculated to be 6.32 eV as shown in Fig. 6b.

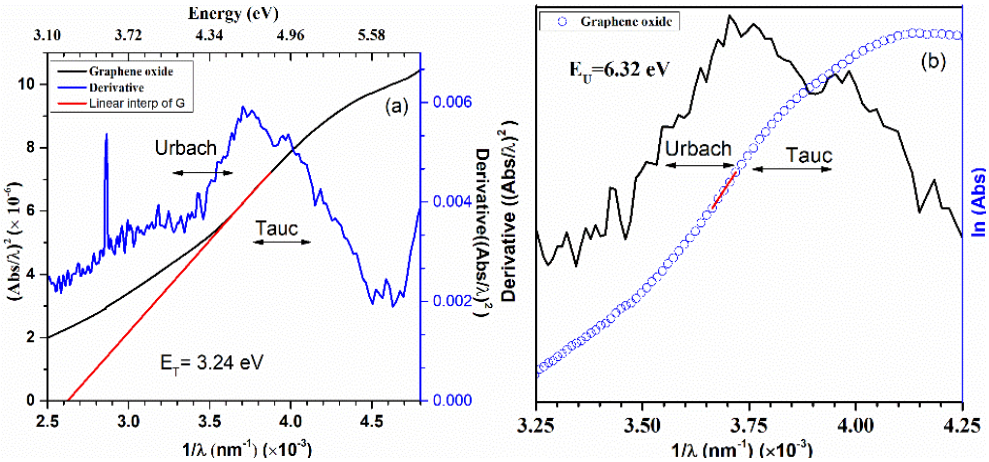

Fig. 6. (a) Bandgap and (b) Urbach energy calculation.

3.5. Raman spectroscopy of graphene oxide

Fig. 7 shows the Raman spectra of graphene oxide at different laser power. Qualitatively, two peaks at 1350 and 1580 cm^{-1} and a broad peak at 2700 cm^{-1} can be observed. Fig. 7b-f shows the deconvolution of the Raman spectra of graphene oxide measured at different laser powers.

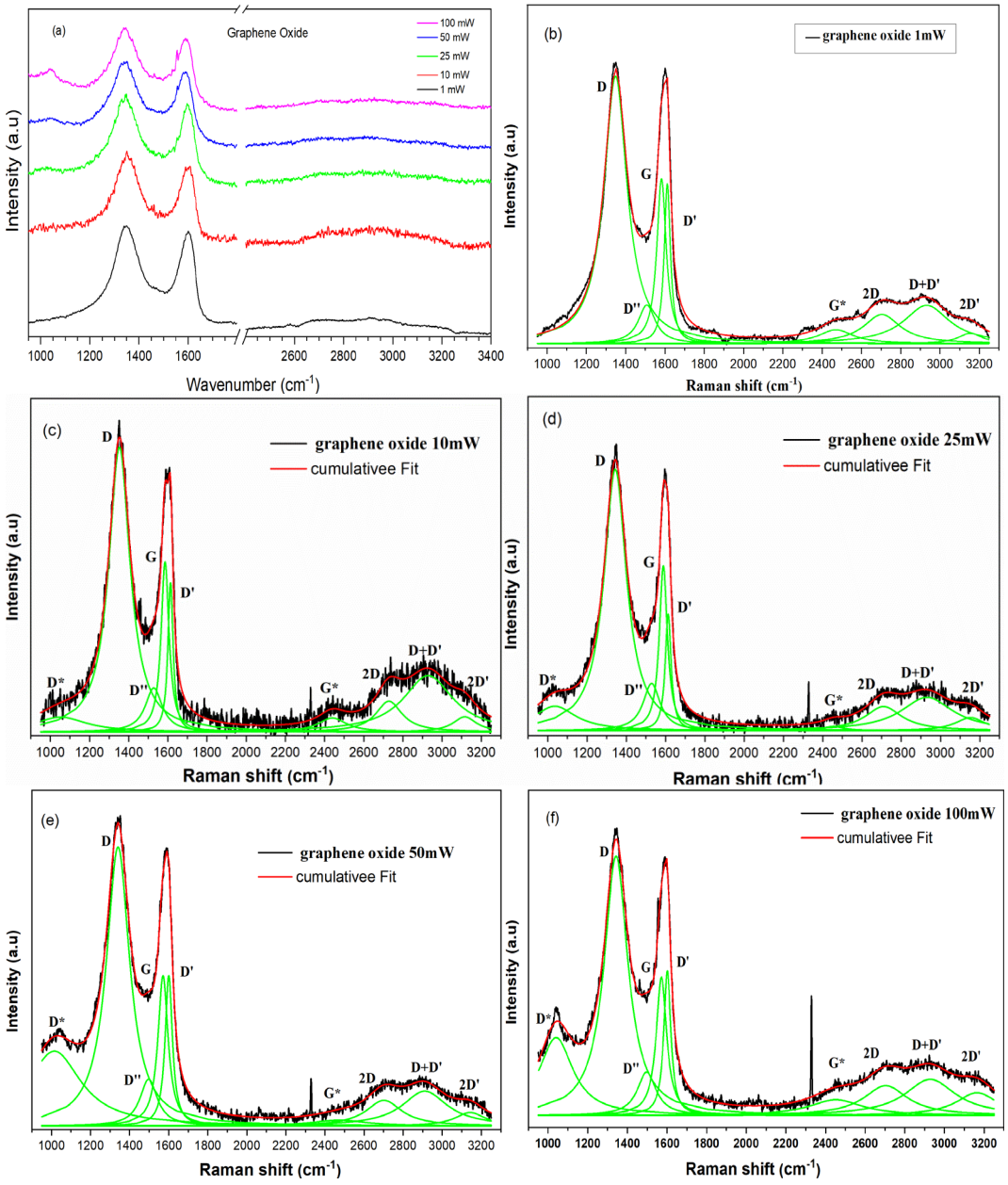

Fig. 7. (a)Raman Spectra of Graphene oxide at different power and Deconvoluted Raman spectra of Graphene oxide at (b) 1 mW, (c) 10 mW, (d)25 mW, (e) 50 mW, and (f) 100 mW laser power for 2 s.

The first and second-order Raman spectra of graphene oxide are fitted using five and four Lorentzian functions, respectively. For the Raman spectra at 1mW, the first order fit requires only four Lorentzian functions, namely D, D", G and D" modes.

4. Discussion

Fig. 8a shows the peak positions of defect modes of first-order Raman spectra of graphene oxide. The D* mode, centered at 1052 cm^{-1} at 10 mW, shifts to a lower wavenumber to 1035 cm^{-1}, 1015 cm^{-1} for 25mW and 50mW, respectively, and shifts to 1040 cm^{-1} for 100mW laser power. A similar dispersive pattern is observed for D, D", G, and D modes. For the D mode, the peak position occurs at 1348 cm^{-1} at 1mW, 1352 cm^{-1} at 10mW, 1343 cm^{-1} at 25mW, 1341 cm^{-1} at 50mW, and 1343 cm^{-1} at 100 mW.

The D" mode shifts from 1508 cm^{-1} at 1 mW to 1528 cm^{-1} at 25 mW, reaching the lowest 1497 cm^{-1} at both 50 mW and 100 mW. The G mode occurs at 1582 cm^{-1} at 1 mW, shifts to 1585 cm^{-1} at 10 mW, 1588 cm^{-1} to 25 mW, lowers to 1570 cm^{-1} at 50 mW, and slightly increases to 1571 cm^{-1} at 100 mW. The D' mode, which occurs along with the G mode, follows a similar pattern, occurs at 1612 cm^{-1} at 1 mW, increases to 1613 cm^{-1} at 10 mW, 1613 cm^{-1} at 25 mW, shifts lower to 1600 cm^{-1} and 1601 cm^{-1} at 100 mW. It can be observed that the peaks shift to the lowest for 50 mW laser power. The standard deviation for the peak positions is 15.4 cm^{-1} for D*, 4.6 cm^{-1} for D, 15.5 cm^{-1} for D", 7.9 cm^{-1} for G and 6.5 cm^{-1} respectively. It shows the dispersion in peak positions is high for D* and D" modes and low for D and G bands. Fig. 8c shows the Full Width at Half maximum (FWHM) values with laser power, indicating a high dispersion for the D* mode with the other modes having low dispersion. The standard deviation for the FWHM is 57.7 cm^{-1} for D*, 5.3 cm^{-1} for D mode, 4.0 cm^{-1} for D" mode, 7.1 cm^{-1} for G mode, and 5.2 cm^{-1} for D' mode. Similarly, the Second order deconvoluted mode shows a higher dispersion in position and FWHM than the first-order modes. The standard deviation for peak position are 13.3 cm^{-1} for G*, 11.0 cm^{-1} for 2D , 8.8 cm^{-1} for D+D’ and 18.3 cm^{-1} for the 2D’ mode. For the FWHM of second-order modes, the standard deviation is 96.5 cm^{-1} for G*, 37.7 cm^{-1} for 2D, 18.5 cm^{-1} for D+D', and 43.7 cm^{-1} for the 2D' mode. The intensities of the individual modes are in arbitrary units; hence, the intensity ratio of different defect modes with the G mode is opted to quantify the defects and the changes in the defect modes in the graphene oxide. Fig. 8e shows the intensity ratio of first-order modes, for 1 mW to 100 mW, the intensity ratio variation of 0 to 0.5 for D*, 1.6 to 1.9 for D, 0.2 to 0.3 for D", and 0.9 to 1.0 for D' mode. Similarly, the Fig. 8f shows the intensity ratio variation for second-order modes, for 1 mW to 100 mW, 0.002 to 0.008, 0.14 to 0.21, 0.20 to 0.33, and 0.06 to 0.16 for G*, 2D, D+D' and 2D' modes, respectively. For both the First and Second order, the intensity ratio is low at 25 mW power and gradually increases to maximum value till 100 mW.

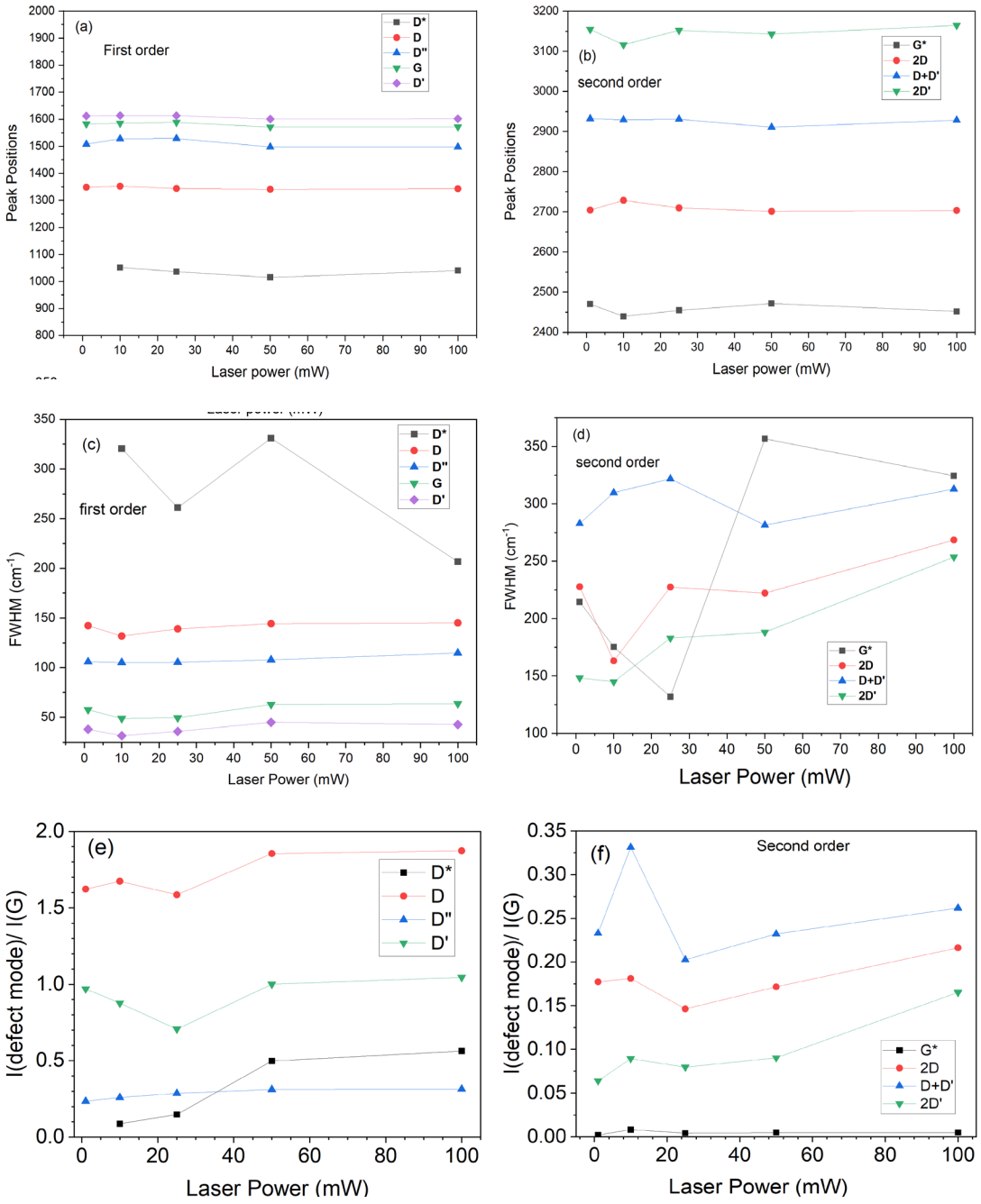

Fig. 8. (a-b) Peak positions, (c-d) Full width at half maxima, (e-f) I(defect mode)/I(G) of first and second-order Raman spectra of graphene oxide at different laser powers for 2s.

The in-plane crystallite size La was calculated using the Tunistra-Kronig model [25,26], and Fig. 9a shows the variation of La with Laser power. The value of La is a maximum of 12.2 nm at 25 mW and reaches a low value of 10.4 nm and 10.3 nm at 50 mW and 100 mW, respectively. Fig. 9b shows the variation of edge defects, sp3 defects, and hopping-like defects with laser power. Using the intensity ratios of $I_D/I_{D'}$, I_D/I_{D*}, and $I_D/I_{D''}$, the edge defects, the sp^3 defects, and the hopping-like defects in the graphene oxide are quantified, respectively. [18]. Fig. 9b shows the quantity of sp^3 defects reduced on the graphene oxide plane with laser power till 50 mW and gets saturated, leading to the formation of reduced graphene oxide. The edge defects in graphene oxide increase with laser power till 25 mW due to a decrease in the in-plane crystallite size; however, the edge defects in graphene oxide decrease partially at 50 mW and get saturated till 100 mW in

proportion to the La values. Similarly, Hopping-defects decrease in graphene oxide till 25 mW of power and slightly increase at 50 mW, and remain saturated till 100 mW of laser power.

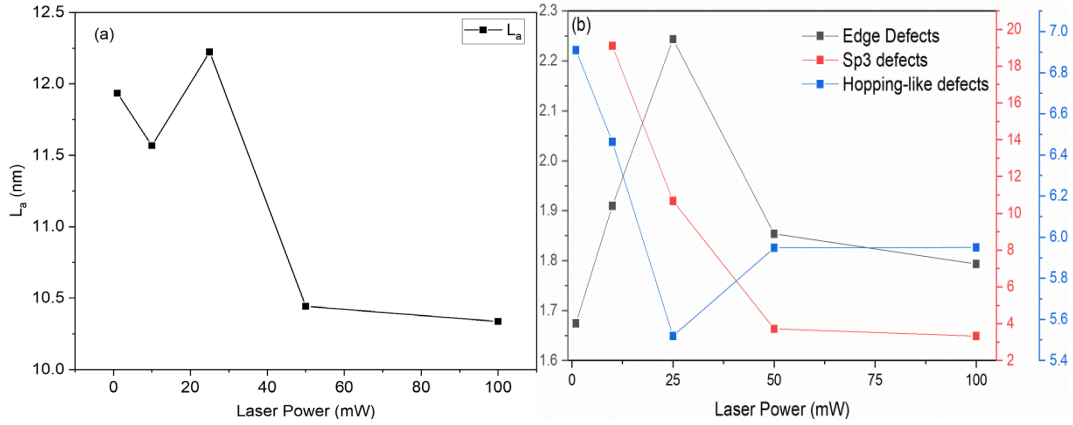

Fig. 9. (a) Variation of In-plane crystallite size L_a and (b) variation of edge, sp^3, and hopping-like defects with laser power.

Fig. 10 shows the variation of $D'_{inf} - G_{app}$ with laser power for different accumulation times of 2 and 5 seconds on graphene oxide. The $D'_{inf} - G_{app}$ increases with the laser power, reaching a maximum value at a laser power of 100 mW for different durations, respectively. King et al. reported vbthree regions based on the $D'_{inf} - G_{app}$ value viz. < 0 ; 0-25 and > 25, correlated to the C/O ratio of < 10; 10-500; and > 500 for GO, rGO, and graphene, respectively [11]. A positive slope of $D'_{inf} - G_{app}$ for all time durations ,indicates the reduction of GO, and at a laser power of 100mW for 5 sec transformed to rGO. The current authors have studied Fourier transform Infrared spectroscopy of similar graphene oxide and shown the presence of the carbonyl (C=O), aromatic (C=C), stretching of the epoxy group (C-O), and C-OH groups in the range of 1010-1740 cm^{-1} [27]. The laser power exposure for an extensive duration causes heating of the surfaces to temperatures up to 150-200 °C, leading to the pyrolysis of the functional groups causing a reduction of graphene oxide.

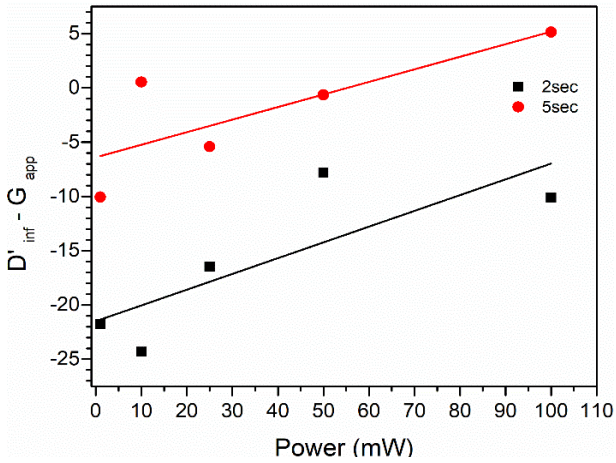

Fig. 10. $D'_{inf} - G_{app}$ at different laser power for different exposure time durations.

4. Conclusions

In summary, graphene oxide is synthesized via the Improved Hummer's method and studied its structural, morphological, thermal, and optical properties. The Raman spectroscopy is utilized at various powers for different exposure time durations to track the changes in the deconvoluted defect modes in the first and second order. The correlations between the in-plane crystallite size L_a, variations in edge defects, sp^3 defects, hopping-like defects, and degree of reduction of graphene oxide are studied. The results are beneficial in tuning the type of defects in the graphene oxide. Further research is needed to formulate a relation between power and duration of exposure to the in-plane crystallite size.

Acknowledgments

The author KLN acknowledges UGC-startup UGC-SRG/30-456/2018(BSR), and GITAM. The authors acknowledge the UGC-NRC, School of Physics, UOH for the facilities provided, and SY acknowledges Dr. M.V.V.S Murthi Research fellowship, GITAM (Deemed to be University).

References

[1] A. Rose, K. Guru Prasad, T. Sakthivel, V. Gunasekaran, T. Maiyalagan, T. Vijayakumar, Applied Surface Science 449, 551 (2018); https://doi.org/10.1016/j.apsusc.2018.02.224

[2] H.-J. Lee and J.-G. Yook, Materials 12, 952 (2019); https://doi.org/10.3390/ma12060952

[3] W. Fan, Y. H. Lee, S. Pedireddy, Q. Zhang, T. Liu, X. Y. Ling, Nanoscale 6, 4843 (2014); https://doi.org/10.1039/C3NR06316J

[4] M. Jin, H.-K. Jeong, W. J. Yu, D. J. Bae, B. R. Kang, Y. H. Lee, J. Phys. D: Appl. Phys. 42, 135109 (2009); https://doi.org/10.1088/0022-3727/42/13/135109

[5] H. Su, Y. H. Hu, Energy Science & Engineering 9, 958 (2021); https://doi.org/10.1002/ese3.833

[6] H. Chen, Y. Yang, D. T. Boyle, Y. K. Jeong, R. Xu, L. S. de Vasconcelos, Z. Huang, H. Wang, H. Wang, W. Huang, H. Li, J. Wang, H. Gu, R. Matsumoto, K. Motohashi, Y. Nakayama, K. Zhao, Y. Cui, Nat Energy 6, 790 (2021); https://doi.org/10.1038/s41560-021-00833-6

[7] A. M. Díez-Pascual, J. A. Luceño Sánchez, R. Peña Capilla, P. García Díaz, Polymers 10, 217 (2018); https://doi.org/10.3390/polym10020217

[8] Y. Wei, Z. Pastuovic, T. Murphy, D. B. Gore, Applied Surface Science 505, 144651 (2020); https://doi.org/10.1016/j.apsusc.2019.144651

[9] A. Cuesta, P. Dhamelincourt, J. Laureyns, A. Martínez-Alonso, J. M. D. Tascón, J. Mater. Chem. 8, 2875 (1998); https://doi.org/10.1039/a805841e

[10] G. A. Zickler, B. Smarsly, N. Gierlinger, H. Peterlik, O. Paris, Carbon 44, 3239 (2006); https://doi.org/10.1016/j.carbon.2006.06.029

[11] A. A. K. King, B. R. Davies, N. Noorbehesht, P. Newman, T. L. Church, A. T. Harris, J. M. Razal, A. I. Minett, Sci Rep 6, 19491 (2016); https://doi.org/10.1038/srep19491

[12] L. G. Cançado, A. Jorio, E. H. M. Ferreira, F. Stavale, C. A. Achete, R. B. Capaz, M. V. O. Moutinho, A. Lombardo, T. S. Kulmala, A. C. Ferrari, Nano Lett. 11, 3190 (2011); https://doi.org/10.1021/nl201432g

[13] A. Y. Lee, K. Yang, N. D. Anh, C. Park, S. M. Lee, T. G. Lee, M. S. Jeong, Applied Surface Science 536, 147990 (2021); https://doi.org/10.1016/j.apsusc.2020.147990

[14] M. A. Pimenta, G. Dresselhaus, M. S. Dresselhaus, L. G. Cançado, A. Jorio, R. Saito, Phys. Chem. Chem. Phys. 9, 1276 (2007); https://doi.org/10.1039/B613962K

[15] D. López-Díaz, J. A. Delgado-Notario, V. Clericò, E. Diez, M. D. Merchán, M. M. Velázquez, Coatings 10, 524 (2020); https://doi.org/10.3390/coatings10060524

[16] D. López-Díaz, M. López Holgado, J. L. García-Fierro, M. M. Velázquez, J. Phys. Chem. C 121, 20489 (2017); https://doi.org/10.1021/acs.jpcc.7b06236

[17] R. Muzyka, S. Drewniak, T. Pustelny, M. Chrubasik, G. Gryglewicz, Materials 11, 1050 (2018); https://doi.org/10.3390/ma11071050

[18] T. Tene, M. Guevara, A. Valarezo, O. Salguero, F. Arias Arias, M. Arias, A. Scarcello, L. S. Caputi, C. Vacacela Gomez, Nanomaterials 11, 1035 (2021); https://doi.org/10.3390/nano11041035

[19] S. Claramunt, A. Varea, D. López-Díaz, M. M. Velázquez, A. Cornet, A. Cirera, J. Phys. Chem. C 119, 10123 (2015); https://doi.org/10.1021/acs.jpcc.5b01590

[20] A. Kaniyoor, S. Ramaprabhu, AIP Advances 2, 032183 (2012); https://doi.org/10.1063/1.4756995

[21] D. C. Marcano, D. V. Kosynkin, J. M. Berlin, A. Sinitskii, Z. Sun, A. Slesarev, L. B. Alemany, W. Lu, J. M. Tour, ACS Nano 4, 4806 (2010); https://doi.org/10.1021/nn1006368

[22] S. N. Alam, N. Sharma, L. Kumar, Graphene 06, 1 (2017); https://doi.org/10.4236/graphene.2017.61001

[23] F. Farivar, P. Lay Yap, R. U. Karunagaran, D. Losic, C 7, 41 (2021); https://doi.org/10.3390/c7020041

[24] N. Ghobadi, Int Nano Lett 3, 2 (2013); https://doi.org/10.1186/2228-5326-3-2

[25] L. G. Cançado, K. Takai, T. Enoki, M. Endo, Y. A. Kim, H. Mizusaki, A. Jorio, L. N. Coelho, R. Magalhães-Paniago, M. A. Pimenta, Appl. Phys. Lett. 88, 163106 (2006); https://doi.org/10.1063/1.2196057

[26] M. Gomaa, G. Abdel Fattah, Appl. Phys. A 126, 519 (2020); https://doi.org/10.1007/s00339-020-03710-3